The epigenetic evolution of gliomas is determined by their IDH1 mutation status and treatment regimen

Tathiane M Malta[1,29], Thais S Sabedot[2,29], Indrani Datta[2,30], Luciano Garofano[3,30], Wies Vallentgoed[4,30], Frederick S Varn[5,30], Kenneth Aldape[6], Fulvio D'Angelo[3], Spyridon Bakas[7,8,9], Jill S Barnholtz-Sloan[6], Hui K Gan[10], Mohammad Hasanain[3], Ann-Christin Hau[11], Kevin C Johnson[5], Mustafa Khasraw[12], Emre Kocakavuk[5], Mathilde CM Kouwenhoven[13], Simona Migliozzi[3], Simone P Niclou[11], Johanna M Niers[13], D. Ryan Ormond[14], Sun Ha Paek[15], Guido Reifenberger[16], Peter A Sillevis Smitt[13], Marion Smits[17,18], Lucy F Stead[19], Martin J van den Bent[13], Erwin G Van Meir[20], Annemiek Walenkamp[21], Tobias Weiss[22], Michael Weller[22], Bart A Westerman[23], Bauke Ylstra[24], Pieter Wesseling[18,24,25], Anna Lasorella[26], Pim J French[4], Laila M Poisson[2], The GLASS Consortium[27], Roel GW Verhaak[5,31], Antonio Iavarone[28,31], Houtan Noushmehr[2,31,*]

1 School of Pharmaceutical Sciences of Ribeirão Preto, University of São Paulo, Ribeirão Preto, São Paulo 14040-900, Brazil

2 Hermelin Brain Tumor Center, Henry Ford Health System, Detroit, MI 48202, USA

3 Institute for Cancer Genetics, Columbia University Medical Center, New York, NY 10032, USA

4 Neurology Department, The Brain tumour center, Erasmus MC Cancer Institute, Rotterdam 3015 GD, the Netherlands

5 The Jackson Laboratory for Genomic Medicine, Farmington, CT 06032, USA

6 National Cancer Institute, Bethesda, MD 20892, USA

7 Center for Biomedical Image Computing and Analytics, University of Pennsylvania, Philadelphia, PA 19104, USA

8 Department of Pathology and Laboratory Medicine, Perelman School of Medicine, University of Pennsylvania, Philadelphia, PA 19104, USA

9 Department of Radiology, Perelman School of Medicine, University of Pennsylvania, Philadelphia, PA 19104, USA

10 Olivia Newton-John Cancer Research Institute, Austin Health, Heidelberg 3084, Melbourne, Australia

11 Luxembourg Institute of Health, Luxembourg L-1526, Luxembourg

12 Duke University, Durham, NC 27710, USA

13 Department of Neurology, Cancer Center Amsterdam, Amsterdam UMC, Vrije Universiteit Amsterdam, 1081 HV Amsterdam, the Netherlands

14 University of Colorado School of Medicine, Department of Neurosurgery, Aurora, CO 80045, USA

15 Seoul National University, Seoul, South Korea

16 Institute of Neuropathology, Heinrich Heine University, Moorenstrasse 5, D-40225 Duesseldorf, Germany

17 Department of Radiology and Nuclear Medicine, Erasmus MC, Rotterdam 3015 GD, the Netherlands

18 The Brain Tumour Centre, Erasmus MC Cancer Institute, Rotterdam, the Netherlands

19 Leeds Institute of Medical Research, University of Leeds, Leeds LS9 7TF, UK

20 Department of Neurosurgery and O'Neal Comprehensive Cancer Center, University of Alabama at Birmingham, Birmingham, AL 35233, USA

21 University of Groningen, Groningen, the Netherlands

22 Department of Neurology, University Hospital and University of Zurich, Frauenklinikstrasse 26, CH-8091 Zurich, Switzerland

23 Department of Neurosurgery, Brain Tumor Center, Cancer Center Amsterdam, Amsterdam UMC, Vrije Universiteit Amsterdam, 1081 HV Amsterdam, the Netherlands

24 Department of Pathology, Cancer Center Amsterdam, Amsterdam UMC, Vrije Universiteit Amsterdam, 1081 HV Amsterdam, the Netherlands

25 Princess Máxima Center for Pediatric Oncology, Utrecht, the Netherlands

26 Department of Pediatrics, Department of Pathology and Cell Biology, Institute for Cancer Genetics, Irving Comprehensive Cancer Center, Columbia University Medical Center, New York, NY 10032, USA

27 A list of participants and their affiliations appears in the online version of the paper

28 Department of Neurology, Department of Pathology and Cell Biology, Institute for Cancer Genetics, Irving Comprehensive Cancer Center, Columbia University Medical Center, New York, NY 10032, USA

29 Co-first author

30 Co-second author

31 Co-senior author

* Correspondence: houtan.noushmehr@hfhs.org

Summary

Tumor adaptation or selection is thought to underlie therapy resistance of gliomas. To investigate the longitudinal epigenetic evolution of gliomas in response to therapeutic pressure, we performed an epigenomic analysis of 143 matched initial and recurrent patients with IDH-wildtype (IDHwt) and IDH-mutant (IDHmut) gliomas. IDHwt gliomas showed a longitudinally stable epigenome with relatively low levels of global methylation, whereas the epigenome of IDHmut gliomas showed initial high levels genome-wide of DNA methylation that was progressively reduced to levels similar to those of IDHwt tumors. By integrating DNA methylation and gene expression data, adaptive changes of putative master regulators of the cell cycle and of differentiation were seen in IDHmut recurrent tumors. Furthermore, relapses of IDHmut tumors were accompanied by histological progression which in turn influenced survival, as validated in an independent cohort. Finally, the initial cell composition of the tumor microenvironment differed between IDHwt and IDHmut tumors and changed differentially following treatment, suggesting increased neo-angiogenesis and T-cell infiltration upon treatment for IDHmut gliomas. Our study provides one of the largest cohorts of paired glioma samples profiled with epigenomics, transcriptomics and genomics; and our results demonstrate that the treatment of IDHmut gliomas reshapes the epigenome towards an IDHwt-like phenotype. Accordingly, the prevalent practice of early genotoxic treatment in this patient population may need to be revisited.

Introduction

Despite advances in our biological understanding, molecular classification and surgical techniques, management of diffuse gliomas of adulthood remains challenging making it an incurable disease (Malta et al., 2018a). Compared to gliomas of the same grade that carry intact isocitrate dehydrogenase (*IDH*) 1 and 2 genes, gliomas with IDH mutations exhibit a less aggressive clinical course which has led to their separation as distinct tumor types in the 2016 World Health Organization (WHO) classification of Tumors of the Central Nervous System (CNS) (Louis et al., 2016). Based on the revised 2021 WHO Classification (Louis et al., 2021), IDH-mutant tumors now comprise two distinct tumor types, namely "oligodendroglioma, IDH-mutant and 1p/19q-codeleted CNS WHO grade 2 or 3", and "astrocytoma, IDH-mutant CNS WHO grade 2, 3 or 4". Yet, there is controversy on the morphological criteria used to distinguish CNS WHO grades 2 and 3, and homozygous *CDKN2A* loss (a signature lesion of CNS WHO grade 4 among IDH-mutant astrocytomas), which is presently the only diagnostic molecular marker in these tumors (Shirahata et al., 2018; Brat et al., 2020; Tesileanu et al., 2021). Thus, additional molecular characterization is needed to establish which of these tumors will rapidly progress or remain quiescent for several years with or without adequate therapy (Weller et al., 2021).

54   Epigenetics play a vital role in stratifying CNS tumors and gliomas into clinically

55 relevant subtypes (Capper et al., 2018; Ceccarelli et al., 2016). The Glioma-CpG Island

56 Methylator Phenotype (G-CIMP) discovered in IDH-mutant gliomas in 2010 (Noushmehr

57 et al., 2010) provided an explanation for their favorable prognosis. Further investigation

58 revealed a subset of IDH-mutant gliomas that presented with a lower degree of DNA

59 methylation and poorer outcome, named G-CIMP-low; distinct from the previously

60 described highly methylated tumors that have a better outcome, and renamed as G-

61 CIMP-high (Ceccarelli et al., 2016). In our previous study, longitudinal epigenomics

62 analyses of 77 paired glioma samples revealed that 12% of G-CIMP-high cases

63 progressed to G-CIMP-low cases (de Souza et al., 2018) highlighting the importance of

64 further studying epigenetic reprogramming following treatment and integrating it with

65 other genomic platforms to discover new prognostic markers and therapeutic targets.

66 Longitudinal analyses that integrate epigenetic and transcriptomic data offer an

67 opportunity to define key master regulators driving the malignant progression of each

68 glioma entity characterizing these prognostic subtypes as tumors transition to

69 recurrence after initial clinical management.

70   Current management and treatment for gliomas include surgery followed by

71 radiotherapy and/or alkylating chemotherapy (e.g. temozolomide [TMZ]). Recent studies

72 have revealed fundamental molecular genetic changes associated with glioma

73 treatment including the development of a hypermutation phenotype (Johnson et al.,

74 2014; Hunter et al., 2006), increase in small deletion burden and acquisition of *CDKN2A*

75 homozygous deletions associated with radiotherapy and acquired aneuploidy

76 associated with cell cycle related genes and overall poorer outcome (Barthel et al.,

77 2019; Kocakavuk et al., 2021). Interestingly, not all TMZ gliomas develop a

78 hypermutator status which challenges the possible mechanisms driving this TMZ

79 treatment-induced molecular phenotype (Mathur et al., 2020; Touat et al., 2020).

80 However, treatment-induced hypermutation related to epigenetic and transcriptomic

81 changes has not been well explored. It offers opportunities to identify potential

82 epigenetic markers for predicting transition to a hypermutator status.

83   In the current study, by leveraging the Glioma Longitudinal AnalySiS (GLASS)

84 international consortium (Barthel et al., 2019; GLASS Consortium, 2018; Varn et al.,

85 2021), we analyze an epigenetic cohort of 143 glioma patients with matched initial and

86 recurrent tumors, and include additional molecular data and clinical data to characterize

87 the evolution of both IDH-wildtype and IDH-mutant gliomas. This is the largest cohort of

88 paired initial and recurrent glioma samples profiled with epigenomics, transcriptomics

89 and genomics, that we know of being used in the literature. Also, the GLASS-NL

90 (GLASS in the Netherlands), a collaboration of several centers in the Netherlands

91 treating patients with glioma, was included in this study to evaluate the effects of

92 treatment in the epigenome of gliomas in an independent cohort. This consortium has

93 collected material from 100 IDH-mutant astrocytoma patients who underwent at least

94 two surgical resections (surgical interval > 6 months). Our study aimed at identifying key

95 master regulators of tumor progression, identifying changes in the tumor

96 microenvironment and epigenetic drivers of glioma evasion to treatment and examining

97 differences in these processes between IDH-wildtype and IDH-mutant gliomas to derive

98 better informed tailored treatments.

Results

Molecular evolution of matched initial and recurrent gliomas

The GLASS-international DNA methylation cohort consists of 143 patients with high-quality molecular data from at least two-time points, resulting in a total of 357 samples profiled by either Illumina 450K or EPIC Beadchip methylation arrays (Tables S1 and S2). The patients at initial diagnosis represented the three major glioma subtypes defined by DNA methylation signatures: IDH-mutant and 1p/19q-co-deleted oligodendroglioma (IDHmut-codel; n = 14); IDH-mutant astrocytoma without 1p/19q co-deletion (IDHmut-noncodel; n = 63); and IDH-wildtype glioblastoma (IDHwt; n = 66). We did not identify samples with IDH2 mutation and thus IDH here represents IDH1 only. Among the 143 patients with profiled DNA methylation, 59 patients had RNA sequencing data, 69 had DNA sequencing genomic data, either whole genome sequencing (WGS) or whole exome sequencing (WXS), and 54 had all three molecular data sets (Figures 1A and S1A). We selected two time-separated tumor samples for each patient, termed initial and recurrence, for further analysis.

To investigate the temporal differences we evaluated the most relevant molecular and clinical features in gliomas. Our cohort includes the previously described DNA methylation-based glioma TCGA subtypes: Three IDH-mut-specific DNA methylation subtypes (Codel, G-CIMP-high, and G-CIMP-low) and three IDHwt-specific subtypes (Classic-like, Mesenchymal-like, LGm6) (Ceccarelli et al., 2016) (Figure 1B) and we used this molecular classification throughout the analyses in this study. Over time, 25% (19/77) of IDHmut and 30% (20/66) of IDHwt tumors switched subtypes. Among IDHmut cases that switched subtypes, tumors of 13 patients (13/19, 68%) switched from G-

5

122 CIMP-high to G-CIMP-low, a subtype associated with worse overall survival (time from

123 initial surgery to death or last follow-up). Among IDHwt cases that switched subtype,

124 tumors of 10 patients (10/20, 50%) switched from classic-like or LGm6 to the

125 mesenchymal-like subtype. Less frequent subtype shifts were also observed. A Pan-

126 CNS DNA methylation-based classification (Heidelberg subtype; Capper et al., 2018)

127 and a recent pathway-based classification of glioblastomas (Functional subtype;

128 Garofano et al., 2021) were also assigned to our cohort (Figure 1B). Based on the Pan-

129 CNS DNA methylation-based classification, 26 IDHmut astrocytomas (26/55, 47%)

130 progressed to high-grade astrocytoma upon recurrence; whereas the IDHwt cases,

131 tumors of 7 patients (7/22, 32%) switched from mesenchymal to RTK II, 6 cases (6/22,

132 27%) switched from RTK II to mesenchymal and 3 (3/9, 33%) from RTK I to

133 mesenchymal.

134 When the patients were stratified according to the genome-wide gain or loss of

135 DNA methylation groups upon recurrence, patients with IDHmut gliomas showed a

136 higher proportion of samples losing DNA methylation than patients with IDHwt gliomas

137 (42% vs 6%; Fisher's test, $p < 0.0001$; Figure 1B). Interestingly, 6 of 8 (75%) of IDHmut

138 tumors that switched molecular subtypes and had genomic data available evidenced

139 hypermutator phenotype at recurrence (Figure 1C, Table S3B). Five of these switched

140 from G-CIMP-high to G-CIMP-low. The tumor of one patient switched from IDHmut

141 Codel to G-CIMP-high (non-codel subtype). In contrast, only 1 of 21 (5%) IDHmut

142 patients which retained their subtype became hypermutator at recurrence (Fisher's test,

143 p=0.0004). All switches were toward a more aggressive phenotype (e.g. G-CIMP-low

144   and grade 4), suggesting an association between DNA methylation change, tumor

145   progression, and hypermutation acquisition.

146   To further explore the association of epigenomic changes and hypermutation, we

147   investigated the methylome of the initial tumors of patients that subsequently received

148   chemotherapy, particularly TMZ, to identify biomarkers that could predict hypermutation

149   in gliomas. We identified 6 IDHmut and 4 IDHwt initial tumors that transformed to

150   hypermutators upon the first recurrence and had treatment information available (Figure

151   S1A). For comparison, we identified 5 IDHmut and 5 IDHwt samples that, despite

152   receiving TMZ and/or RT after initial surgery, did not become hypermutators which were

153   used as controls.

154   A supervised analysis between initial IDHmut gliomas that did or did not develop

155   a hypermutator phenotype at recurrence resulted in 342 differentially methylated CpG

156   probes (unadjusted p-value < 0.01 and DNA methylation difference > 25%) (Figure S1B,

157   Table S5). To understand the biological implications of these DNA methylation changes,

158   we integrated the methylome data with RNA-sequencing and selected CpGs within the

159   promoter region of genes and identified 23 CpG-gene pairs inversely correlated, such

160   as the DNA replication initiator gene *REPIN1* and the gene *KCNK2,* which has been

161   associated with positive regulation of cellular response to hypoxia (Wu et al. 2013),

162   indicating potential mechanisms associated with the predisposition to hypermutation

163   (Figure S1C). Within IDHwt tumors, we identified 548 CpG probes that were associated

164   with hypermutation in IDHwt gliomas (unadjusted p-value < 0.05 and DNA methylation

165   difference > 30%) and 14 genes being negatively correlated with CpG methylation,

166   including *MGMT* and the gene *NETO1*, which is associated with regulation of long-term

167 neuronal synaptic plasticity (Ng et al. 2009) (Figure S1D and S1E, Table S5). Further

168 studies would be needed to confirm the predictive power of these signatures.

169   Despite evidence that hypermutation might occur in random chromosomal

170 locations (Touat et al., 2020), we investigated the methylome of the recurrent

171 hypermutated tumors to identify regions with consistent patterns of DNA methylation.

172 We compared the epigenome between first recurrence hypermutators (N=8 IDHmut; 7

173 IDHwt) and non-hypermutators (N=11 IDHmut; 20 IDHwt), stratified by IDH status. In

174 the IDHmut group, we identified 502 differentially methylated CpG probes (DMP)

175 (unadjusted p-value < 0.01 and DNA methylation difference > 30%) that defined the

176 hypermutator phenotype in gliomas, the majority of which were hypomethylated (Figure

177 S1F, Table S5). In IDHwt tumors, the set of CpG probes identified by our analysis

178 (N=620; unadjusted p-value < 0.05 and DNA methylation difference > 40%) showed that

179 the hypermutators are mostly hypermethylated compared to non-hypermutators

180 (N=94%; 581/620) (Figure S1G, Table S5). Taken together, these findings suggest that

181 epigenetic biomarkers predict the predisposition to hypermutation in patients who

182 receive TMZ after the initial surgery. Further validation studies could help elucidate the

183 biological role of these regions in determining the susceptibility to hypermutation.

184 Master regulators associated with IDHmut glioma progression

185   To further investigate the changes in the epigenome that occur over time in

186 gliomas, we compared the genome-wide DNA methylation characteristics of the initial

187 compared to recurrent tumor samples, stratified by IDH status (Figure S2B). IDHwt

188 gliomas showed a more stable epigenome over time (i.e. zero CpG probes presented a

189 differentially methylated mean difference greater than 20%), while the epigenome of

8

190   IDHmut gliomas showed genome-wide loss of DNA methylation (593 CpG probes with

191   DNA methylation difference > 20%) throughout the disease evolution (Figure S2B).

192   IDHmut patients that progressed from G-CIMP-high to G-CIMP-low showed the most

193   prominent loss of DNA methylation, particularly at intergenic regions, which suggests an

194   association between the loss of DNA methylation and tumor progression in this subtype

195   (Figures S2C, S2D and S2E), confirming previous results from our group and others

196   (Nomura et al., 2019; de Souza et al., 2018). Compared to patients with tumors that

197   remained G-CIMP-high at recurrence, those with recurrent G-CIMP-low more often had

198   histologically higher-grade astrocytoma, were less often managed by a watch-and-wait

199   strategy and exhibited inferior survival (Table S3A).

200   Next, we investigated the impact of the epigenomic changes on transcriptional

201   networks using an integrative approach that combines epigenome and transcriptome to

202   define   master   regulators.   We   applied   ELMER   (Enhancer   Linking   by

203   Methylation/Expression Relationships) (Silva et al., 2019; Yao et al., 2015), a

204   computational tool that harnesses DNA methylation to identify regulatory elements and

205   correlates the enhancer state with the expression of nearby genes to define putative

206   transcriptional targets. ELMER also allows the inference of transcription factor (TF)

207   binding motif analysis and the integration of TF expression to identify master regulatory

208   TFs (MRTFs) (Silva et al., 2019).

209   We compared initial and recurrent IDHmut gliomas and identified a total of 1,590

210   DMP between the groups (FDR < 0.05, Figure 2A, S4A). To better understand the

211   genomic context of the DNA methylation changes associated with the progression of

212   IDHmut gliomas, we profiled nine IDHmut G-CIMP-high gliomas at diagnosis and three

213 recurrences evolving into IDHmut G-CIMP-low states with ChIP-seq for the H3K27Ac

214 active chromatin mark. The integration of DMP with the local changes of H3K27Ac (20

215 nearest genes of each CpG probe in the methylation array) converged on the

216 identification of 1,282 genes exhibiting coordinated loss of DNA methylation and gain of

217 H3K27Ac, thus indicating that this gene set is epigenetically activated by loss of DNA

218 methylation at recurrence. A pathway-based analysis of these genes suggested

219 enrichment of cell cycle and proliferation-related activities (Figure 2B, Table S4B).

220 Within the regulatory DMP regions, we identified the enrichment of 32 distal-

221 binding motifs for specific TFs with TGAGTCA (Fos/Jun family) and the enhancer-box

222 CAGATGG being the most represented (Figure 2A, Table S4C). By computing the

223 anticorrelation of TF gene expression and the DNA methylation levels within their

224 binding sites, we identified candidate TFs with increasing expression in IDHmut

225 recurrent tumors to levels comparable to those of IDHwt gliomas (Figure 2C). Some of

226 these master regulatory (MR) TFs are well-established glioma oncogenes: FOS/JUN

227 family members have been associated with control of tumor malignancy (Blau et al.,

228 2012), cell proliferation and radioresistance (Liu et al., 2016), and glioma progression

229 (de Souza et al., 2018); musculin (MSC) has been reported to inhibit differentiation of

230 embryonal carcinoma (Yu et al., 2003) and B-cell lymphoma cells (Mathas et al., 2006).

231 Indeed, recurrent IDHmut tumors show higher stemness activity (as defined by our

232 recent study) (Malta et al., 2018b) than the corresponding initial tumors (Figure 2D).

233 We also identified 201 DMP between initial and recurrent IDHwt glioma samples,

234 which were mapped to both distal regions (156 CpG probes) and promoters (45 CpG

235 probes) and their putative associated genes (Figure S2F and S2G). We did not identify

236   any TF binding motifs enriched within the DMP regions, showing again less frequent

237   changes in epigenetic regulation in IDHwt tumors over time.

238   Together, our results show that IDHmut gliomas present a more dynamic

239   epigenome, characterized by loss of DNA methylation at recurrence, with activation of

240   oncogenes to expression levels similar to those observed in IDHwt gliomas. In contrast,

241   the epigenome of IDHwt gliomas seems relatively preserved longitudinally. We

242   identified potential master regulators driving cell cycle deregulation in IDHmut gliomas

243   at recurrence, which represent potential treatment targets.

244   DNA methylation loss associated with recurrent IDHmut gliomas after standard

245   treatment

246   It has been shown that treatment (radiotherapy and alkylating chemotherapy) improves

247   the progression-free survival of IDHmut gliomas (Wick et al., 2009). However,

248   recurrence of IDHmut lower-grade glioma is frequently associated with progression to

249   higher histological grades. Treatment of IDHmut lower-grade gliomas with TMZ and/or

250   radiotherapy has been linked to many genomic alterations, such as a hypermutator

251   phenotype (Johnson et al., 2014; Touat et al., 2020), and a strong tendency towards

252   aneuploidy and a specific radiotherapy-associated deletion signature by genetic

253   analysis (Kocakavuk et al., 2021). Herein, we observe that treatment is associated with

254   epigenomic changes. Whether and how to treat a low-grade IDH-mutant glioma is still

255   not based on high level evidence from controlled clinical trials; we sought to identify the

256   DNA methylation changes triggered at recurrence by the different treatment choices

257   made in our cohort. Towards this goal, we divided our cohort into 4 groups: patients

258   who received TMZ only (N=12), radiotherapy (RT) only (N=18), the combination of RT

259   and TMZ (RT+TMZ; N=6) and patients who did not receive additional treatment after the

260   first surgery but were managed by a watch-and-wait approach (N=33) (Tables S3D and

261   S6). The supervised methylome analysis of first recurrent IDHmut gliomas across the 4

262   groups defined 620 DMP (Kruskal-Wallis test by ranks, FDR < 0.01 and DNA

263   methylation difference > 20%) (Figure 3A, Table S6). Upon first investigation, we

264   determined that these CpGs were associated with consistent loss of DNA methylation in

265   patients who received any treatment besides surgery after initial diagnosis (TMZ only,

266   RT only or combined TMZ and RT) compared to their primary counterparts. On the

267   other hand, the methylome of the recurrent sample of patients who did not receive

268   treatment resembled the initial tumor (Figure 3A). There were no CpG probes that

269   distinguished the different groups that received any specific type of treatment (TMZ

270   only, RT only or RT+TMZ), suggesting that the introduction of any treatment regimen

271   involving TMZ and/or RT after initial surgery is sufficient to remodel the methylome of

272   treatment-*naïve* gliomas. The interrogation of the same CpGs corroborated this

273   observation in IDHwt initial and recurrent gliomas, which showed a similar DNA

274   hypomethylation profile to the IDHmut treatment arm (TMZ only, RT only and RT+TMZ)

275   (Figure 3A). To evaluate whether the observed decrease of DNA methylation in our

276   discovery cohort (GLASS-International; this study) is consistent in an independent

277   cohort, we sought to validate our findings in a yet unpublished dataset of paired glioma

278   samples from the GLASS in the Netherlands consortium (GLASS-NL; validation)

279   (GLASS Consortium, 2018). The validation cohort consists of 36 treated paired glioma

280   samples and 64 untreated paired samples, all of which are IDHmut astrocytomas at

281   diagnosis. The loss of DNA methylation pattern upon treatment after initial surgery was

282　confirmed in the validation cohort (Figures 3B and 3C). Because the GLASS-NL cohort

283　was comprised of only IDHmut astrocytomas, we repeated our discovery test on only

284　the IDHmut astrocytomas of the GLASS-International cohort (excluding

285　oligodendroglioma samples), separated by treatment group and selected a new set of

286　DNA hypomethylated CpG probes (N=981) in the treated samples (FDR < 0.01 and

287　DNA methylation difference > 25%). 61% (381/620) of the previously described CpG

288　probe list overlapped with this new signature showing consistent DNA methylation

289　changes. Again, the loss of DNA methylation pattern after treatment was confirmed in

290　the validation cohort (Figure S3A, Table S6).

291　　　By comparing different clinical and molecular features of these tumors, we

292　observed a significant enrichment of progression to IDHmut astrocytoma CNS WHO

293　grade 4 in the treatment vs the non-treatment groups in the discovery (Fisher's test =

294　0.03; Figure 3D) but not with the validation datasets (Fisher's test p = 0.3; Figure S3B).

295　In addition, we noticed that 34% (10/29) of G-CIMP-high tumors progressed to G-CIMP-

296　low in the treatment group vs 4% (1/27) in the non-treatment group (Fisher's test,

297　p=0.005). The same was observed with the molecular Pan-CNS classification (Capper

298　et al., 2018), in which 68% (15/22) of IDHmut astrocytomas progressed to high-grade

299　astrocytoma in the treatment group vs 23% (6/26) in the non-treatment group (Fisher's

300　test, p=0.003, Table S1). As expected, only in the treatment group, we observed

301　hypermutator samples (N=5) (Figure 3A). To consider whether the selection of the

302　treatment regimen might have been biased by the age at diagnosis, we performed an

303　analysis of variance (ANOVA) on age at the initial tumor resection and we did not find

304　an age difference across the four groups (ANOVA F-test p-value = 0.59). To explore the

305   biological implications of these epigenomic changes, we searched for inversely

306   correlated DNA methylation and gene expression. We identified 24 distal CpG-gene

307   pairs (FDR < 0.01) enriched for the NEUROD1 motif resulting in 18 unique genes

308   potentially regulated by DNA methylation after treatment (Figures 3E and S3C, Table

309   S6) which included known oncogenes and cancer-related genes such as MYB and

310   MYO15A and enriched for monocarboxylic acid metabolic process.

311   Tumor microenvironment changes and clinical implications of treatment in IDH-mutant

312   gliomas revealed by DNA methylation

313   As the observed changes of DNA methylation may not only be driven by tumor

314   cell-intrinsic-events but may also underscore changes in the methylome associated with

315   non-tumor cell populations present in the glioma tumor microenvironment (TME), we

316   applied a methylation-specific approach for the deconvolution of non-tumor cells to the

317   longitudinal glioma cohort. MethylCIBERSORT (Chakravarthy et al., 2018) uses

318   genome-wide DNA methylation data to deconvolute cell types from individual tumor

319   samples. Our estimated cell populations consisted of 10 cell types: glia, neuron,

320   endothelial cells (CD31+), B cells (CD19+), CD4 effector T cells, CD8+ T cells, T regs,

321   natural killer cells (CD56+), macrophages and neutrophils. Compared to untreated

322   recurrencies, recurrent IDHmut tumors which were treated after surgery were marked

323   by increased infiltration of endothelial cells (CD31+) and CD8 T lymphocytes (CD8+)

324   (Figure 4A, Table S7), suggesting that treatment impacts the tumor microenvironment

325   and most notably angiogenesis. Our *in silico* cell fraction estimation was validated by

326   immunohistochemical staining in representative IDHmut samples that received

327   treatment after initial surgery (Figure 4B). As a further validation, the relative proportion

328   of non-tumor cells estimated by methylCIBERSORT was significantly correlated with the

329   glioma cell compartments estimated by gene expression for the GLASS-international

330   transcriptomic cohort (Varn et al., 2021) (Figure S4A). Additional changes in the TME

331   were also observed within IDHmut and IDHwt longitudinally, particularly a significant

332   increase in macrophage in recurrent IDHwt tumors (Figures S4B-S4D).

333   To evaluate the clinical implications of these findings, we next assessed the

334   clinical follow-up of the entire IDHmut GLASS-International cohort divided into treatment

335   (N=73) or non-treatment (N=37) groups. First, patients receiving treatment after initial

336   surgery had a worse survival than patients who did not receive treatment beyond

337   surgery (log-rank p-value=0.03, Figure 4C, left). However, patients left untreated after

338   initial surgery had a progression-free interval (PFI) of 27 months that was significantly

339   worse compared to a PFI of 40.5 months in the treatment group (log-rank p=0.009,

340   Figure 4C, middle), thus confirming the results of EORTC 22845 (van den Bent et al.,

341   2005). When we focused on the survival interval from second surgery to the last follow-

342   up, as expected, we found a markedly worse survival in previously treated patients (log-

343   rank p=0.0001, Figure 4C, right). The same associations of treatment and clinical

344   implications were observed in the validation GLASS-NL cohort (Figure 4D).

345

Discussion

347   This work reports and analyzes the largest cohort of matched glioma samples

348   profiled with epigenomics, transcriptomics, and genomics platforms to uncover the

349   diverse molecular routes that drive treatment-resistant gliomas during progression. By

350 applying an integrative molecular approach, we highlight the critical epigenetic

351 mechanisms by which gliomas evaded treatment in addition to transcriptomic and

352 genetic evolution. We also identified epigenomic changes that may be useful as

353 biomarkers for continuous monitoring of disease progression and treatment response

354 prediction.

355   Our cohort consisted of the three major glioma subtypes (IDHmut-noncodel,

356 IDHmut-codel and IDHwt) and revealed key evolutionary differences across these

357 subgroups. Earlier work from us and others described the G-CIMP glioma phenotype in

358 IDHmut glioma characterized by higher levels of DNA methylation likely as a direct

359 result of the epigenetic effects of the oncometabolite 2-hydroxyglutarate that is

360 generated by mutant IDH enzymes (Noushmehr et al., 2010; Turcan et al., 2012).

361 These tumors exhibited favorable clinical outcomes compared with IDHwt gliomas,

362 which have lower DNA methylation levels (Noushmehr et al., 2010). Indeed, in our

363 previous work, we reported that the extent of genome-wide DNA methylation showed

364 broad positive correlation with clinical outcome for IDHwt glioma, now defined as

365 "molecular GBM" given their aggressive behavior independent of histological grading

366 (Louis et al., 2001), with these tumors having the lowest levels of DNA methylation

367 genome-wide. Here we confirm and extend these notions to tumor progression. In

368 particular, we found that IDHwt gliomas presented an initial low genome-wide DNA

369 methylation, which shows minimal changes during the course of the disease. This is

370 consistent with the malignant state of IDHwt gliomas at diagnosis and which does not

371 appear to progress during treatment.

372   Conversely, we uncovered pronounced epigenetic changes in IDHmut gliomas,

373   which invariably converged toward lower DNA methylation levels in recurrent treated

374   tumors compared to untreated neoplasms. In the most extreme cases, the treatment-

375   induced evolution of IDHmut glioma resulted in a state of DNA hypomethylation

376   comparable to IDHwt gliomas. Thus, the epigenetic trajectory of glioma progression was

377   associated with progressively lower levels of DNA methylation in IDHmut tumors or was

378   essentially moot in the case of IDHwt gliomas as glioma initiation in the absence of IDH

379   mutations coincided with the lowest possible levels of DNA methylation.

380   Following diagnosis and surgery, IDHmut glioma patients may or may not

381   undergo treatment with radiation or alkylating chemotherapy or both (Baumert et al.,

382   2016; Buckner et al., 2016). A recognized effect of alkylating agents typically used in

383   glioma therapy (temozolomide) is the potential acquisition of a hypermutator phenotype

384   (Barthel et al., 2019; Johnson et al., 2014). Here, we found that treatment with radiation

385   and/or chemotherapy individually or combined accelerated progression towards the

386   hypomethylated state at recurrence. These findings were confirmed in an independent

387   cohort, suggesting that current treatment regimens alter the epigenomic landscape of

388   IDHmut gliomas similar to the observed treatment-induced genomic abnormalities in

389   response to alkylating agents.

390   The treatment-accelerated epigenetic drift towards the hypomethylated state

391   parallels the histopathological shift from a lower- to a higher-grade phenotype.

392   Altogether, these results indicate that the initial treatment with radiotherapy and/or

393   temozolomide may have triggered a more aggressive evolution at the time of the tumor

394   recurrence which compromised the survival probability of these patients at that

395 recurrence. More specifically, the introduction of treatment after initial surgery in IDH-

396 mutant gliomas is associated with a significant delay in tumor progression. The time

397 from second surgery to progression or death is significantly shorter when compared to

398 untreated patients which is likely associated with the loss of DNA methylation and

399 activation of associated genes that we uncovered. While these findings remain

400 consistent with previous observations from large clinical trials that reported the

401 beneficial role of chemotherapy and radiotherapy for patients survival (van den Bent et

402 al., 2005), they also highlight the ability of radio/chemotherapy to trigger a markedly

403 more aggressive behavior at recurrence and identify the epigenetic determinants of the

404 treatment-induced glioma progression.

405   The therapy-associated changes of the epigenetic evolution of IDHmut glioma

406 were also mirrored by specific changes in the tumor microenvironment (TME) at

407 recurrence. At recurrence, CD8 and endothelial cell-related signatures were elevated in

408 treated IDHmut gliomas compared to untreated tumors. Together, these findings

409 indicate that the epigenomic and genomic changes associated with more aggressive

410 histotypes of IDHmut gliomas at recurrence coincided with specific changes of the TME

411 (neo-angiogenesis and changes in T-cell composition), indicating the convergence of

412 IDHmut glioma evolution towards features more typical to the most aggressive IDHwt

413 subtype.

414   Having established the importance of epigenetic evolution of IDHmut glioma, we

415 focused on this subtype to integrate the analysis of epigenome, transcriptome and

416 ChIP-seq to extract the features associated with the evolution towards loss of DNA

417 methylation and consequent transcriptional activation of critical drivers of progression

18

418   (master regulators, MRs). First, the integration of DNA methylation and transcriptomic

419   platforms uncovered the convergence towards gene sets enriched with cell cycle and

420   proliferation-related activities and stemness, in comparison to initial tumors. Thus, such

421   biological activities are directly activated by transcriptional derepression associated with

422   local loss of DNA methylation. Second, we focused our attention on identifying MRs that

423   enabled the biological evolution of IDHmut glioma. MR are TFs regulating multiple

424   genes and in the case of cancer, drive the onset or progression of the disease.

425   Our approach depends on our understanding that discrete regions of the genome

426   harbors DNA sequence elements recognized by TFs. The presence of the TF and the

427   accessibility of the functional elements can then drive the activity of nearby or distant

428   genes. We uncovered a set of established oncogenes as MRs activated by

429   hypomethylation-induced derepression in IDHmut glioma, among them FOS/JUN family

430   members. Interestingly, therapeutic targeting of cJun transcription has included small

431   molecules interfering with its DNA binding domain, thereby preventing it from activating

432   downstream target genes such as those represented in our study. Two such molecules

433   with potential therapeutic advantages are MLN944 (Dai et al., 2004) and retinoid

434   (SR11302) which could be explored in a follow-up study involving recurrent glioma

435   tumors.

436   In summary, we found that upon tumor progression after standard treatment loss

437   of DNA methylation in IDHmut tumors is frequent which results in epigenetic activation

438   of cell cycle-related genes associated with early tumor progression and alterations in

439   the TME contexture towards angiogenesis and a T-cell composition that resembles a

440   treatment-naive IDHwt glioma (Figure 5). In untreated IDHmut patients the epigenome

19

441   does not change significantly, and tumors progress later than the treated ones, either

442   spontaneously or after subsequent treatment.

443

Figure Legends:

444

445   **Figure 1. Epigenomic evolution of matched initial and recurrent gliomas. A)** Venn diagram
446   of number of patients who had DNA methylation, genomic (WGS/WXS) and/or RNAseq
447   profiling. **B)** Clinical and molecular overview of matched initial and recurrent DNA methylation
448   cohort. Each column represents a single patient (n=143) at two separate time points grouped by
449   IDH status and ordered by increase of gain of DNA methylation at recurrent tumor from left-to-
450   right. Top plot shows the surgical interval of each patient. **C)** Frequency of patients with
451   hypermutator tumors that switched or retained molecular subtype at recurrence. Patients are
452   divided by IDH status.

453

454   **Figure 2. Master regulators associated with IDHmut glioma recurrence/progression. A)**
455   Circos plot diagram showing epigenomic changes between initial and recurrent IDHmut tumors.
456   The outer track shows chromosome location. The second track shows genomic location of
457   1,590 differentially methylated CpG probes between initial and recurrent IDHmut tumors. Height
458   of dots represents the difference of methylation levels between recurrent and initial. The third
459   track shows the genomic location of H3H27ac peaks defined by differential binding analysis of
460   IDHmut G-CIMP-high patients that progressed to G-CIMP-low. Height of the peaks represents
461   the fold change of differential binding analysis. The fourth inner track shows the genomic
462   location of the candidate genes epigenetically regulated by the CpG probes (yellow bars).
463   Height of the bars represents the -log of FDR. Genes related to cell cycle are labeled. The top
464   transcription factor (TF) binding motifs enriched among the candidate DMP are FOS/JUN family
465   and NEUROD1, whose DNA signature motifs are represented in the center of the circos plot. **B)**
466   Pathway analysis of epigenetically activated genes in recurrent IDHmut tumors. **C)** Gene
467   expression levels of master regulator transcription factors (MRTFs) of IDHmut initial and
468   recurrent tumors. IDHwt tumors are shown as a reference. **D)** Stemness activity in glioma
469   samples stratified by primary/recurrent and IDH mutation status.

470

471   **Figure 3. DNA methylation loss associates with malignant transformation of glioma after**
472   **standard treatment. A)** Heatmap of DNA methylation data. Supervised hierarchical clustering
473   analysis of 620 CpG probes that are associated with different treatment strategies in IDH-
474   mutant paired glioma samples. Columns represent glioma samples, rows represent CpG
475   probes. Samples were stratified and clustered based on IDH mutation status and
476   primary/recurrent status and CpGs were ordered using hierarchical clustering methods. Non-
477   neoplastic brain samples are represented on the left of the heatmap. DNA methylation beta-

478 values range from 0 (low) to 1 (high). Additional tracks are included at the top of the heatmaps
479 to identify each sample membership within separate cluster analysis. **B)** Heatmap of DNA
480 methylation data in the validation cohort - GLASS-NL, showing the same 620 CpG probes of
481 panel A. **C)** Boxplot of the average DNA methylation beta-value of the 620 CpG probes from
482 panel A. Samples are stratified by primary/recurrent status and by treated/non-treated status.
483 Left: GLASS-International samples. Right: GLASS-NL samples. **D)** Evolution of tumor histology
484 (2021 WHO classification) from primary to recurrent samples after treatment compared to non-
485 treated gliomas. **E)** Scatter plot of mean DNA methylation of CpG probes and mean gene
486 expression of the epigenetically regulated genes after treatment.

488 **Figure 4. Tumor microenvironment and clinical implications of treatment in IDH-mutant**
489 **gliomas. A)** CD31 and CD8 proportions (range scaled from 0 to 100%) in samples originating
490 from IDHmut matched initial and recurrent tumors in treated and non-treated patients. **B)**
491 Illustrative immunohistochemical stainings for two marker proteins (CD31 and CD8) in an
492 individual patient showing change of levels of tumor-infiltrating immune cells between initial and
493 recurrent tumors. **C/D)** Overall survival and surgical interval analysis of IDHmut gliomas for the
494 GLASS International (C) and GLASS-NL (D) cohorts.

496 **Figure 5. Schematic of treatment-induced epigenetic activation of cell cycle in IDHmut**
497 **recurrent tumors.** Standard treatment induces loss of methylation in IDHmut tumors with
498 further epigenetic activation of cell cycle related genes associated with early tumor progression.
499 In IDHmut non-treated patients, epigenetic changes are much more limited and tumors may
500 progress later, either spontaneously or after subsequent treatment.

Supplemental Figure Legends:

503 **Figure S1: DNA methylation signature to predict the hypermutator phenotype upon initial**
504 **surgery divided by IDH status, related to Figure 1. A)** Venn diagram of the GLASS
505 hypermethylator cohort based on data type: Whole-genome sequencing, DNA methylation array
506 and clinical follow-up. **B)** Heatmap of DNA methylation data across IDHmut samples at initial
507 diagnosis that were treated with TMZ, stratified by hypermutator status. Supervised hierarchical
508 clustering analysis of 342 CpG probes that can predict the hypermutator status at the initial
509 surgery. Column-wise represents 11 glioma samples, row-wise represents CpG probes.
510 Samples and CpGs are ordered using hierarchical clustering method. DNA methylation beta-
511 values range from 0 (low) to 1 (high). Additional tracks are included at the top of the heatmaps
512 to identify each sample membership within separate cluster analysis. **C)** Boxplot of the CpG-
513 gene pairs at gene promoter regions of IDHmut gliomas divided by DNA methylation (top) and
514 gene expression (bottom) data. **D)** DNA methylation heatmap of 548 CpG data across IDHwt
515 samples at initial diagnosis treated with TMZ, stratified by hypermutator status. **E)** Boxplot of
516 CpG-gene pairs at gene promoter regions identified in IDHwt gliomas. **F/G)** Differentially
517 methylated regions between hypermutator vs non-hypermutator recurrent samples divided by
518 IDH status: F, IDHmut and G, IDHwt.

520 **Figure S2. Longitudinal epigenomic changes of matched initial and recurrent gliomas,**
521 **related to Figure 2. A)** Venn diagram of DNA methylation samples which were profiled with
522 genomics (WGS/WXS) and/or RNAseq. **B)** Overall genome-wide DNA methylation correlation
523 between initial and recurrent tumors, stratified by IDH mutation status. **C/D/E)** Overall DNA
524 methylation correlation between initial and recurrent tumors of different glioma subtypes, by
525 CpG probe genomic location: C, genome-wide; D, probes located in intergenic regions, and E,
526 CpG probes located in promoters of genes. **F/G)** Differentially methylated CpG probes defined
527 between recurrent and initial IDHwt tumors and their associated putative genes. F, CpG probes
528 located at distal regions and G, CpG probes located at promoter regions.

529

530 **Figure S3. DNA methylation loss is associated with malignant progression of glioma after**
531 **standard treatment in the validation cohort: GLASS-NL, related to Figure 3. A)** Heatmap of
532 DNA methylation data. Supervised analysis using astrocytoma-only samples from GLASS-
533 International cohort identified 981 CpG probes that are associated with treatment astrocytomas
534 IDHmut paired glioma samples. Samples from the validation cohort are also shown. Samples
535 are stratified by cohort, initial/recurrent status and treatment status. Column-wise represents
536 glioma samples, row-wise represents CpG probes. DNA methylation beta-values range from 0
537 (low) to 1 (high). Additional tracks are included at the top of the heatmaps to identify each
538 sample membership within separate cluster analysis. **B)** Evolution of tumor histology (2021
539 WHO classification) of the validation cohort (GLASS-NL) after treatment compared to non-
540 treated gliomas. **C)** Scatter plot of 24 CpG-gene pairs epigenetically regulated genes after
541 treatment in IDHmut gliomas.

542

543 **Figure S4. Glioma subtypes present different tumor microenvironments and it changes**
544 **overtime, related to Figure 4. A)** Correlation between cell composition estimated by DNA
545 methylation and by gene expression. **B)** Barplots of the estimated median infiltration of specific
546 cell types as a proportion of all cell types (range scaled from 0 to 100%) in 143 glioma tumors at
547 initial diagnosis, divided by IDH mutation status. **C)** Cell type proportion (range scaled from 0 to
548 100%) in samples originating from the matched initial and recurrent tumors, divided by
549 molecular subtypes. All comparisons (initial vs. recurrence, by subtype, for the specified cell
550 population) are statistically significant (P < 0.05). P values calculated using a two-sided
551 Wilcoxon rank-sum test. Matched primary and recurrent tumors are linked by the lines. **D)**
552 Representative immunohistochemical staining for CD163 marker protein in two individual
553 patients with changing levels of tumor-infiltrating immune cells between initial and recurrent
554 tumors.

555

556

557

558

559

560

Methods

562

CONTACT FOR REAGENT AND RESOURCE SHARING

Further information and requests for resources and reagents should be directed to and will be fulfilled by the Lead Contact Houtan Noushmehr (hnoushm1@hfhs.org).

566

Biospecimens/GLASS Datasets

Datasets added to GLASS came from both published and unpublished sources. The GLASS epigenomic cohort consists of 357 DNA methylation samples (143 patients) profiled by either Illumina 450K or EPIC Beadchip methylation arrays and described below. For those same patients, we also collected DNA sequencing data of 157 genomic samples, WXS or WGS (69 patients); and RNA sequencing of 120 samples (59 patients), available through the GLASS consortium, resulting in the largest cohort of matched glioma samples profiled with epigenomics, transcriptomics and genomics platforms.

Newly generated DNA methylation data was collected from four different institutions: Henry Ford Hospital (n=103), University of Leeds (UK) (n= 8), Chinese University of Hong Kong (n=6), and Luxembourg Institute of Health (n=54). The DNA was extracted at each institution. New DNA methylation data from Henry Ford Hospital and from Chinese University of Hong Kong was generated at the University of Southern California. Briefly, the DNA was bisulfite-converted (Zymo EZ DNA methylation Kit; Zymo Research) and profiled using an Illumina Human EPIC array (EPIC). For the Luxembourg Institute of Health samples, DNA methylation data was generated by the Illumina EPIC array at the Helmholtz Zentrum München (Research Unit of Molecular Epidemiology, Institute of Epidemiology, German Research Center for Environmental Health, Neuherberg, Germany) or by the Laboratoire National de Santé (Neuropathology Unit, National Center of Pathology, Dudelange, Luxembourg). Samples from University of Leeds were profiled locally using Illumina 450K Beadchip

589 methylation arrays. The raw DNA methylation intensity data files (IDAT) were processed
590 with the minfi package (Fortin et al., 2017). We performed noob (Normal-exponential
591 convolution using out-of-band probes) background correction (Triche et al., 2013) and
592 dye bias correction using the minfi package (v 1.36.0) (Fortin et al., 2017). The DNA
593 methylation value for each locus is presented as a beta (β) value (β = (M/(M+U)) in
594 which M and U indicate the mean methylated and unmethylated signal intensities for
595 each locus, respectively. β-values range from zero to one, with scores of zero indicating
596 no DNA methylation and scores of one indicating complete DNA methylation. A
597 detection p-value also accompanies each data point and compares the signal intensity
598 difference between the analytical probes and a set of negative control probes on the
599 array. Any data point with a corresponding p-value greater than 1E-4 is deemed not to
600 be statistically significantly different from background and was thus masked as "NA". All
601 data   files   that   were   used   in   our   analysis   can   be   found   at
602 https://www.synapse.org/#!Synapse:syn17038081/wiki/585622.

603 RNA expression data used in this study was downloaded from the GLASS portal and
604 the TPM data matrix was filtered for selected protein coding genes only. Next, batch
605 effects due to the different Aliquot Batches were corrected using the COMBAT algorithm
606 with aliquots as covariates (Leek et al., 2012).

607 Public Datasets

608 Public samples included in the GLASS cohort were downloaded from: TCGA/GDC
609 (https://portal.gdc.cancer.gov), (Bai et al., 2016; Mazor et al., 2015, 2017; de Souza et
610 al., 2018). The raw DNA methylation IDAT files were accessed and processed as
611 described for the GLASS datasets above. Sample IDs and tissue source sites from our
612 entire longitudinal glioma cohort are listed in Table S1.

613 Quality control

614 DNA methylation quality control was performed using the entire GLASS epigenetic
615 samples to ensure the identity check of samples matched to their corresponding patient.
616 The DNA methylation signals of probes querying high-frequency SNPs were used to
617 calculate a pairwise agreement score across samples (Heiss and Just, 2018). Only

618 samples that passed our pairwise agreement score cutoff were kept in the GLASS
619 epigenetic cohort (n=357).

Classification of longitudinal gliomas

621 Longitudinal glioma samples were classified as either IDH-wildtype (Classic-like,
622 Mesenchymal-like, LGm6) or IDH-mutant (Codel, G-CIMP-high, and G-CIMP-low) DNA
623 methylation subtypes using the CpG methylation signatures and method previously
624 defined by our group (Ceccarelli et al., 2016).
625 Our cohort was also classified into the Pan-CNS DNA methylation-based classification
626 (Capper et al., 2018) by uploading idat files into the portal
627 https://www.molecularneuropathology.org/mnp.
628 Additionally, the samples were classified into the recent transcriptomic pathway-based
629 classification of glioblastomas (Garofano et al., 2021) using MWW-GST on the basis of
630 the highest positive Normalized Enrichment Score (Frattini et al. 2018).
631 Hypermutation was defined for all recurrent tumors that had received TMZ after initial
632 surgery and had more than 10 mutations per megabase sequenced, as described
633 previously (Barthel et al., 2019).

Identification of master regulator transcription factors

635 Initial and recurrent glioma samples were compared using the package ELMER (Silva et
636 al., 2019) for the following pair-wise comparison: IDHmut initial vs recurrent (20
637 matched pairs), IDHwt initial vs recurrent (29 pairs), and IDHmut treated vs untreated
638 (20 matched pairs). Only samples that have both DNA methylation and gene expression
639 available were used in these analyses.
640 We applied the default probe filter "distal," which uses 158,803 probes that are >2 kbp
641 from any transcription start site as annotated by GENCODE. ELMER version 2.14 was
642 used with the following parameters: get.diff.meth(sig.diff) = 0, get.diff.meth(p_value) =
643 0.05, get.diff.meth (minSubgroupFrac) = 0.2, get.pair(Pe) = 0.1, get.pair(raw.pvalue) =
644 0.05, get.pair(filter.probes) = FALSE, get.pair(diff.dir)=both, get.pair(permu.size) = 100,
645 get.pair(minSubgroupFrac) = 0.4, get.enriched.motif(lower.OR) = 1.1,
646 get.enriched.motif(min.incidence) = 2. For each comparison, the TF subfamilies were

25

647 inferred from the TFs, which had the most significant anticorrelation scores. The
648 candidate MRTFs were next identified within the TF subfamily with FDR < 0.05 using
649 the classification from TFClass.

Supervised analysis associated with treatment

651 Only patients with known TMZ and RT treatment status after initial surgery were
652 included in the supervised analysis. In total, we identified 6 patients who received both
653 TMZ and RT, 12 patients who received only TMZ, 18 patients who received RT only and
654 33 patients who did not receive additional treatment besides surgery. We used the
655 Kruskal–Wallis test by ranks followed by multiple testing using the Benjamini &
656 Hochberg (BH) method for false discovery rate (FDR) estimation (Benjamini et al.,
657 2001) to identify differentially methylated sites between these four groups at first
658 recurrence. To define significant CpG probes, we selected probes with FDR < 0.01 and
659 mean DNA methylation difference > 20%.

660 We investigated the association of differentially methylated CpG probes (FDR < 0.01; N
661 = 5,218 CpG probes) with gene expression from 6 untreated and 14 treated (TMZ, RT
662 and TMZ+RT) first recurrent samples with available DNA methylation and RNA-
663 sequencing data using ELMER and filtering by distal probes (Silva et al., 2019). Finally,
664 we applied the function "get.enriched.motif" with only "A" motif quality score (highest
665 confidence) to identify CpG-gene pairs enriched for the same DNA motif signature. The
666 CpG probes and genes of interest identified by these analyses were then sent to our
667 collaborators who are part of the GLASS-NL consortium for validation of our results.

DNA methylation and gene expression data from the GLASS-NL cohort

669 The GLASS-NL consortium has collected material from 100 IDH-mutant astrocytoma
670 (1p19q non-codeleted) patients who underwent at least two surgical resections. Material
671 for analysis had to be available for both resections, and the surgical interval between
672 resections was > 6 months. Detailed clinical data, imaging, and treatment data of
673 patients was collected within the consortium. All institutions obtained ethics approval
674 from their institutional review boards or ethics review committees before initiation of the

675 project. All patients provided written informed consent according to local and national
676 guidelines.

677 DNA and RNA were isolated from formalin-fixed paraffin-embedded (FFPE) tumour
678 samples as previously described (Draaisma et al., 2020). Evaluation of the area with
679 highest tumor content was done by the pathologist (PW) on a hematoxylin and eosin
680 stained section. Macrodissection of the marked area was then done on 10-20 10µm
681 consecutive slides. DNA and RNA extraction was performed using the QIAamp DNA
682 FFPE and RNeasy FFPE kit respectively (both Qiagen, Venlo, The Netherlands). DNA
683 methylation profiling was performed with the Infinium MethylationEPIC BeadChip
684 according to the manufacturer's instructions making use of the Infinium FFPE DNA
685 Restoration Kit. RNA-sequencing was done by Genomescan (Leiden, the Netherlands)
686 and data processing, alignment and further analysis of read counts was done as
687 described (Hoogstrate et al., 2020).

688 ## Deconvolution analysis

689 We first constructed a signature matrix from reference DNA methylation profiles of pure
690 flow-sorted populations of cells from the literature. This signature matrix represents a
691 set of differentially methylated CpGs selected and weighted to reflect specificity for a
692 given cell type and is used as the basis of cell deconvolution by methylCIBERSORT.
693 Our final signature matrix consisted of 10 cell types: CD19+ cells (B cells) (n=6), CD8+
694 T cells (n=6), CD56+ (natural killer cells) (n=6), and neutrophils (n=12) were from the
695 FlowSorted.Blood.450k Bioconductor package version 1.30.0 (Reinius et al., 2012).
696 CD4+ effector T cells (n=6) and T regs (n=4) were from (Zhang et al., 2013), accessed
697 through the MethylCIBERSORT R package (Chakravarthy et al., 2018). Vascular
698 endothelial cells (n=2) data was from (Moss et al., 2018). Monocyte-derived
699 macrophage (n=4) data was from (Dekkers et al., 2019). Neuron (n=31) and glia cells
700 (n=31) were from (Gasparoni et al., 2018). The MethylCIBERSORT R package was
701 used to derive the DNA methylation signature for the deconvolution and the signature
702 matrix was exported and uploaded to the CIBERSORTx portal to be deconvoluted using
703 1000 permutations without quantile normalization.

704

705 Validation of tumor cell composition

706   Sections of formalin-fixed, paraffin-embedded human glioma surgical samples

707 were deparaffinized with xylene and rehydrated through graded alcohol into deionized

708 H_2O. Antigens were unmasked by incubation for 45 mins at 95°C in Diva Decloaker

709 (Biocare, DV2004) using Biocare's Decloaking chamber, and sections were stained with

710 the antibodies listed on the table, visualized with intelliPATH FLX™ DAB Chromogen Kit

711 (Biocare, IPK5010) and counterstained with intelliPATH™ Hematoxylin (Biocare,

712 IPCS5006L). The antibodies are listed in the Key Resource Table.

713   Images of the tissue sections stained by immunohistochemistry using CD163,

714 CD31, and CD8 antibodies were captured by an Olympus IX70 microscope and a digital

715 camera. For quantitative analysis, we selected eight representative areas in each

716 section. Images of the representative areas were captured at a 10X magnification. For

717 CD163 and CD31 stainings, individual cells per area were identified by strong brown

718 stain and counted by using ImageJ (NIH, Bethesda USA) by an algorithm to evaluate

719 staining using hematoxylin and DAB staining specific built-in color deconvolution plug-

720 in. For CD8 immunostaining, positive cells identified in each area by strong brown stain

721 were manually counted. The cell counting was repeated three times. All images were

722 analyzed in a blinded fashion. Values are presented as mean±standard deviation.

723 Groups were compared and potential differences were identified using the non-

724 parametric t test.

725

726 Statistical analysis

727 Data visualization and statistical analysis were performed using R version 4.1.0

728 software packages (www.r-project.org) and Bioconductor (Gentleman et al., 2004).

729 Unless specified, significance was access with an FDR adjustment of less than 5%.

730

731 Code and data availability

732 Processed data for the GLASS consortium is available on Synapse
733 (https://www.synapse.org/#!Synapse:syn21589818) and will be publicly available on
734 November 9, 2021.

735 Acknowledgements

749

750

751

752   KEY RESOURCE TABLE

REAGENT or RESOURCE	SOURCE	IDENTIFIER
Software and Algorithms		
MethylCIBERSORT	(Chakravarthy et al., 2018)	https://doi.org/10.5281/zenodo.1298968
CIBERSORTx	(Newman et al., 2019)	https://cibersortx.stanford.edu/
R version 4.0.5	(R Core Team, 2017)	https://www.R-project.org
minfi (v1.36.0)	(Aryee et al., 2014)	https://bioconductor.org/packages/release/bioc/html/minfi.html
TCGAbiolinks (v2.18.0)	(Colaprico et al., 2016)	http://bioconductor.org/packages/TCGAbiolinks/
ELMER (v2.14.0)	(Silva et al., 2019)	http://bioconductor.org/packages/ELMER/
DNA methylation-based classification of central nervous system tumors	(Capper et al., 2018)	https://www.molecularneuropathology.org/mnp
CD8	Rabbit Monoclonal (C8/1779R)	Biocare, API3219AA
CD31	Mouse Monoclonal (BC2)	Biocare, PM347
CD163	Mouse Monoclonal (10D6)	Biocare, PM353AA
Deposited Data		
Raw DNA methylation data	This paper	
TCGA data	NIH Genomic Data Commons (GDC)	https://gdc.cancer.gov/about-data/publications/PanCanStemness-2018
Published longitudinal glioma cohort	(Mazor et al., 2015)	EGAS00001001255

Published longitudinal glioma cohort	(Mazor et al., 2017)	EGAS00001001854
Published longitudinal glioma cohort	(Bai et al., 2016)	EGAS00001001588
Neuron and glia cells data	(Gasparoni et al., 2018)	GSE66351
Blood cells (CD19+, CD8+ T, CD56+, neutrophils	(Reinius et al., 2012)	GSE35069
CD4+ effector T and T regs	(Zhang et al., 2013)	GSE49667
Vascular endothelial cells	(Moss et al., 2018)	GSE122126
Monocyte-derived macrophage	(Dekkers et al., 2019)	GSE118696

753

754
755

756 **Author Contributions:**

757

758 Conceptualization, T.M.M., T.S.S., R.G.W.V., A.I., H.N.;

759 Methodology, T.M.M., T.S.S., H.N.;

760 Formal Analysis, T.M.M., T.S.S., I.D., W.V., L.G., P.J.F.;

761 Investigation, T.M.M., T.S.S.;

762 Resources, T.M.M., T.S.S., F.S.V.;

763 Data curation, T.M.M, T.S.S, I.D., F.S.V., L.G., W.V., K.A., L.D., S.B., J.S.B., H.K.G., M.H.,

764 A.C.H., K.C.J, M.K., E.K., M.C.M.K., S.M., S.P.N., J.M.N., D.R.O., S.H.P., G.R., P.A.S.S., M.S.,

765 L.F.S., M.J.V.D.B., E.G.V.M., A.W., T.W., M.W., B.A.W., B.Y., P.W., A.L., P.J.F., L.M.P.,

766 R.G.W.V., A.I., H.N.;

767 Writing- Original draft, T.M.M., T.S.S., H.N., A.I.;

768 Writing-Review & Editing, T.M.M, T.S.S, I.D., F.S.V., L.G., W.V., K.A., L.D., S.B., J.S.B., H.K.G.,

769 M.H., A.C.H., K.C.J, M.K., E.K., M.C.M.K., S.M., S.P.N., J.M.N., D.R.O., S.H.P., G.R., P.A.S.S.,

770 M.S., L.F.S., M.J.V.D.B., E.G.V.M., A.W., T.W., M.W., B.A.W., B.Y., P.W., A.L., P.J.F., L.M.P.,

771 R.G.W.V., A.I., H.N.;

772 Funding acquisition, H.N., L.M.P., R.G.W.V.;

773 Supervision, H.N., A.I., R.G.W.V.

774

775 All co-authors and contributors discussed the results and commented on the manuscript.

776

777

778

779

780

781

782

783

784

785

786

787

788

789

790

791

Bibliography

Aryee, M.J., Jaffe, A.E., Corrada-Bravo, H., Ladd-Acosta, C., Feinberg, A.P., Hansen, K.D., and Irizarry, R.A. (2014). Minfi: a flexible and comprehensive Bioconductor package for the analysis of Infinium DNA methylation microarrays. Bioinformatics *30*, 1363–1369.

Bai, H., Harmancı, A.S., Erson-Omay, E.Z., Li, J., Coşkun, S., Simon, M., Krischek, B., Özduman, K., Omay, S.B., Sorensen, E.A., et al. (2016). Integrated genomic characterization of IDH1-mutant glioma malignant progression. Nat. Genet. *48*, 59–66.

Barthel, F.P., Johnson, K.C., Varn, F.S., Moskalik, A.D., Tanner, G., Kocakavuk, E., Anderson, K.J., Abiola, O., Aldape, K., Alfaro, K.D., et al. (2019). Longitudinal molecular trajectories of diffuse glioma in adults. Nature *576*, 112–120.

Baumert, B.G., Hegi, M.E., van den Bent, M.J., von Deimling, A., Gorlia, T., Hoang-Xuan, K., Brandes, A.A., Kantor, G., Taphoorn, M.J.B., Hassel, M.B., et al. (2016). Temozolomide chemotherapy versus radiotherapy in high-risk low-grade glioma (EORTC 22033-26033): a randomised, open-label, phase 3 intergroup study. Lancet Oncol. *17*, 1521–1532.

Benjamini, Y., Drai, D., Elmer, G., Kafkafi, N., and Golani, I. (2001). Controlling the false discovery rate in behavior genetics research. Behav. Brain Res. *125*, 279–284.

Blau, L., Knirsh, R., Ben-Dror, I., Oren, S., Kuphal, S., Hau, P., Proescholdt, M., Bosserhoff, A.-K., and Vardimon, L. (2012). Aberrant expression of c-Jun in glioblastoma by internal ribosome entry site (IRES)-mediated translational activation. Proc Natl Acad Sci USA *109*, E2875-84.

Brat, D.J., Aldape, K., Colman, H., Figrarella-Branger, D., Fuller, G.N., Giannini, C., Holland, E.C., Jenkins, R.B., Kleinschmidt-DeMasters, B., Komori, T., et al. (2020). cIMPACT-NOW update 5: recommended grading criteria and terminologies for IDH-mutant astrocytomas. Acta Neuropathol. *139*, 603–608.

Buckner, J.C., Shaw, E.G., Pugh, S.L., Chakravarti, A., Gilbert, M.R., Barger, G.R., Coons, S., Ricci, P., Bullard, D., Brown, P.D., et al. (2016). Radiation plus Procarbazine, CCNU, and Vincristine in Low-Grade Glioma. N. Engl. J. Med. *374*, 1344–1355.

Capper, D., Jones, D.T.W., Sill, M., Hovestadt, V., Schrimpf, D., Sturm, D., Koelsche, C., Sahm, F., Chavez, L., Reuss, D.E., et al. (2018). DNA methylation-based classification of central nervous system tumours. Nature *555*, 469–474.

Ceccarelli, M., Barthel, F.P., Malta, T.M., Sabedot, T.S., Salama, S.R., Murray, B.A., Morozova, O., Newton, Y., Radenbaugh, A., Pagnotta, S.M., et al. (2016). Molecular profiling reveals biologically discrete subsets and pathways of progression in diffuse glioma. Cell *164*, 550–563.

Chakravarthy, A., Furness, A., Joshi, K., Ghorani, E., Ford, K., Ward, M.J., King, E.V., Lechner, M., Marafioti, T., Quezada, S.A., et al. (2018). Pan-cancer deconvolution of tumour composition using DNA methylation. Nat. Commun. *9*, 3220.

830 Colaprico, A., Silva, T.C., Olsen, C., Garofano, L., Cava, C., Garolini, D., Sabedot, T.S., Malta,
831 T.M., Pagnotta, S.M., Castiglioni, I., et al. (2016). TCGAbiolinks: an R/Bioconductor package for
832 integrative analysis of TCGA data. Nucleic Acids Res. *44*, e71.

833 Dai, J., Punchihewa, C., Mistry, P., Ooi, A.T., and Yang, D. (2004). Novel DNA bis-intercalation
834 by MLN944, a potent clinical bisphenazine anticancer drug. J. Biol. Chem. *279*, 46096–46103.

835 Dekkers, K.F., Neele, A.E., Jukema, J.W., Heijmans, B.T., and de Winther, M.P.J. (2019).
836 Human monocyte-to-macrophage differentiation involves highly localized gain and loss of DNA
837 methylation at transcription factor binding sites. Epigenetics Chromatin *12*, 34.

838 Draaisma, K., Chatzipli, A., Taphoorn, M., Kerkhof, M., Weyerbrock, A., Sanson, M., Hoeben,
839 A., Lukacova, S., Lombardi, G., Leenstra, S., et al. (2020). Molecular Evolution of IDH Wild-
840 Type Glioblastomas Treated With Standard of Care Affects Survival and Design of Precision
841 Medicine Trials: A Report From the EORTC 1542 Study. J. Clin. Oncol. *38*, 81–99.

842 Frattini, V., Pagnotta, S.M., Tala, Fan, J.J., Russo, M.V., Lee, S.B., Garofano, L., Zhang, J., Shi,
843 P., Lewis, G., et al. (2018). A metabolic function of FGFR3-TACC3 gene fusions in cancer.
844 Nature 553, 222–227.

845 Fortin, J.-P., Triche, T.J., and Hansen, K.D. (2017). Preprocessing, normalization and
846 integration of the Illumina HumanMethylationEPIC array with minfi. Bioinformatics *33*, 558–560.

847 Garofano, L., Migliozzi, S., Oh, Y.T., D'Angelo, F., Najac, R.D., Ko, A., Frangaj, B., Caruso,
848 F.P., Yu, K., Yuan, J., et al. (2021). Pathway-based classification of glioblastoma uncovers a
849 mitochondrial subtype with therapeutic vulnerabilities. Nat. Cancer *2*, 141–156.

850 Gasparoni, G., Bultmann, S., Lutsik, P., Kraus, T.F.J., Sordon, S., Vlcek, J., Dietinger, V.,
851 Steinmaurer, M., Haider, M., Mulholland, C.B., et al. (2018). DNA methylation analysis on
852 purified neurons and glia dissects age and Alzheimer's disease-specific changes in the human
853 cortex. Epigenetics Chromatin *11*, 41.

854 Gentleman, R.C., Carey, V.J., Bates, D.M., Bolstad, B., Dettling, M., Dudoit, S., Ellis, B.,
855 Gautier, L., Ge, Y., Gentry, J., et al. (2004). Bioconductor: open software development for
856 computational biology and bioinformatics. Genome Biol. *5*, R80.

857 GLASS Consortium (2018). Glioma through the looking GLASS: molecular evolution of diffuse
858 gliomas and the Glioma Longitudinal Analysis Consortium. Neuro Oncol. *20*, 873–884.

859 Heiss, J.A., and Just, A.C. (2018). Identifying mislabeled and contaminated DNA methylation
860 microarray data: an extended quality control toolset with examples from GEO. Clin. Epigenetics
861 *10*, 73.

862 Hoogstrate, Y., Vallentgoed, W., Kros, J.M., de Heer, I., de Wit, M., Eoli, M., Sepulveda, J.M.,
863 Walenkamp, A.M.E., Frenel, J.-S., Franceschi, E., et al. (2020). EGFR mutations are associated
864 with response to depatux-m in combination with temozolomide and result in a receptor that is
865 hypersensitive to ligand. Neurooncol Adv *2*, vdz051.

866 Hunter, C., Smith, R., Cahill, D.P., Stephens, P., Stevens, C., Teague, J., Greenman, C.,
867 Edkins, S., Bignell, G., Davies, H., et al. (2006). A hypermutation phenotype and somatic MSH6
868 mutations in recurrent human malignant gliomas after alkylator chemotherapy. Cancer Res. *66*,
869 3987–3991.

870 Johnson, B.E., Mazor, T., Hong, C., Barnes, M., Aihara, K., McLean, C.Y., Fouse, S.D.,
871 Yamamoto, S., Ueda, H., Tatsuno, K., et al. (2014). Mutational analysis reveals the origin and
872 therapy-driven evolution of recurrent glioma. Science *343*, 189–193.

873 Kocakavuk, E., Anderson, K.J., Varn, F.S., Johnson, K.C., Amin, S.B., Sulman, E.P., Lolkema,
874 M.P., Barthel, F.P., and Verhaak, R.G.W. (2021). Radiotherapy is associated with a deletion
875 signature that contributes to poor outcomes in patients with cancer. Nat. Genet. *53*, 1088–1096.

876 Leek, J.T., Johnson, W.E., Parker, H.S., Jaffe, A.E., and Storey, J.D. (2012). The sva package
877 for removing batch effects and other unwanted variation in high-throughput experiments.
878 Bioinformatics *28*, 882–883.

879 Liu, Z.-G., Jiang, G., Tang, J., Wang, H., Feng, G., Chen, F., Tu, Z., Liu, G., Zhao, Y., Peng, M.-
880 J., et al. (2016). c-Fos over-expression promotes radioresistance and predicts poor prognosis in
881 malignant glioma. Oncotarget *7*, 65946–65956.

882 Louis, D.N., Perry, A., Reifenberger, G., von Deimling, A., Figarella-Branger, D., Cavenee,
883 W.K., Ohgaki, H., Wiestler, O.D., Kleihues, P., and Ellison, D.W. (2016). The 2016 World Health
884 Organization Classification of Tumors of the Central Nervous System: a summary. Acta
885 Neuropathol. *131*, 803–820.

886 Louis, D.N., Perry, A., Wesseling, P., Brat, D.J., Cree, I.A., Figarella-Branger, D., Hawkins, C.,
887 Ng, H.K., Pfister, S.M., Reifenberger, G., et al. (2021). The 2021 WHO Classification of Tumors
888 of the Central Nervous System: a summary. Neuro Oncol.

889 Malta, T.M., de Souza, C.F., Sabedot, T.S., Silva, T.C., Mosella, M.S., Kalkanis, S.N., Snyder,
890 J., Castro, A.V.B., and Noushmehr, H. (2018a). Glioma CpG island methylator phenotype (G-
891 CIMP): biological and clinical implications. Neuro Oncol. *20*, 608–620.

892 Malta, T.M., Sokolov, A., Gentles, A.J., Burzykowski, T., Poisson, L., Weinstein, J.N., Kamińska,
893 B., Huelsken, J., Omberg, L., Gevaert, O., et al. (2018b). Machine Learning Identifies Stemness
894 Features Associated with Oncogenic Dedifferentiation. Cell *173*, 338-354.e15.

895 Mathas, S., Janz, M., Hummel, F., Hummel, M., Wollert-Wulf, B., Lusatis, S., Anagnostopoulos,
896 I., Lietz, A., Sigvardsson, M., Jundt, F., et al. (2006). Intrinsic inhibition of transcription factor
897 E2A by HLH proteins ABF-1 and Id2 mediates reprogramming of neoplastic B cells in Hodgkin
898 lymphoma. Nat. Immunol. *7*, 207–215.

899 Mathur, R., Zhang, Y., Grimmer, M.R., Hong, C., Zhang, M., Bollam, S., Petrecca, K., Clarke, J.,
900 Berger, M.S., Phillips, J.J., et al. (2020). MGMT promoter methylation level in newly diagnosed
901 low-grade glioma is a predictor of hypermutation at recurrence. Neuro Oncol. *22*, 1580–1590.

902 Mazor, T., Pankov, A., Johnson, B.E., Hong, C., Hamilton, E.G., Bell, R.J.A., Smirnov, I.V.,
903 Reis, G.F., Phillips, J.J., Barnes, M.J., et al. (2015). DNA methylation and somatic mutations
904 converge on the cell cycle and define similar evolutionary histories in brain tumors. Cancer Cell
905 *28*, 307–317.

906 Mazor, T., Chesnelong, C., Pankov, A., Jalbert, L.E., Hong, C., Hayes, J., Smirnov, I.V.,
907 Marshall, R., Souza, C.F., Shen, Y., et al. (2017). Clonal expansion and epigenetic
908 reprogramming following deletion or amplification of mutant IDH1. Proc Natl Acad Sci USA *114*,
909 10743–10748.

910   Moss, J., Magenheim, J., Neiman, D., Zemmour, H., Loyfer, N., Korach, A., Samet, Y., Maoz,
911   M., Druid, H., Arner, P., et al. (2018). Comprehensive human cell-type methylation atlas reveals
912   origins of circulating cell-free DNA in health and disease. Nat. Commun. *9*, 5068.

913   Newman, A.M., Steen, C.B., Liu, C.L., Gentles, A.J., Chaudhuri, A.A., Scherer, F., Khodadoust,
914   M.S., Esfahani, M.S., Luca, B.A., Steiner, D., et al. (2019). Determining cell type abundance and
915   expression from bulk tissues with digital cytometry. Nat. Biotechnol. *37*, 773–782.

916   Ng, D., Pitcher, G.M., Szilard, R.K., Sertié, A., Kanisek, M., Clapcote, S.J., Lipina, T., Kalia,
917   L.V., Joo, D., McKerlie, C., et al. (2009). Neto1 is a novel CUB-domain NMDA receptor-
918   interacting protein required for synaptic plasticity and learning. PLoS Biol. 7, e41.

919   Nomura, M., Saito, K., Aihara, K., Nagae, G., Yamamoto, S., Tatsuno, K., Ueda, H., Fukuda, S.,
920   Umeda, T., Tanaka, S., et al. (2019). DNA demethylation is associated with malignant
921   progression of lower-grade gliomas. Sci. Rep. *9*, 1903.

922   Noushmehr, H., Weisenberger, D.J., Diefes, K., Phillips, H.S., Pujara, K., Berman, B.P., Pan, F.,
923   Pelloski, C.E., Sulman, E.P., Bhat, K.P., et al. (2010). Identification of a CpG island methylator
924   phenotype that defines a distinct subgroup of glioma. Cancer Cell *17*, 510–522.

925   Reinius, L.E., Acevedo, N., Joerink, M., Pershagen, G., Dahlén, S.-E., Greco, D., Söderhäll, C.,
926   Scheynius, A., and Kere, J. (2012). Differential DNA methylation in purified human blood cells:
927   implications for cell lineage and studies on disease susceptibility. PLoS ONE *7*, e41361.

928   R Core Team, R.C.T. (2017). R: A language and environment for statistical computing (Vienna,
929   Austria: R Foundation for Statistical Computing).

930   Shirahata, M., Ono, T., Stichel, D., Schrimpf, D., Reuss, D.E., Sahm, F., Koelsche, C., Wefers,
931   A., Reinhardt, A., Huang, K., et al. (2018). Novel, improved grading system(s) for IDH-mutant
932   astrocytic gliomas. Acta Neuropathol. *136*, 153–166.

933   Silva, T.C., Coetzee, S.G., Gull, N., Yao, L., Hazelett, D.J., Noushmehr, H., Lin, D.-C., and
934   Berman, B.P. (2019). ELMER v.2: an R/Bioconductor package to reconstruct gene regulatory
935   networks from DNA methylation and transcriptome profiles. Bioinformatics *35*, 1974–1977.

936   de Souza, C.F., Sabedot, T.S., Malta, T.M., Stetson, L., Morozova, O., Sokolov, A., Laird, P.W.,
937   Wiznerowicz, M., Iavarone, A., Snyder, J., et al. (2018). A Distinct DNA Methylation Shift in a
938   Subset of Glioma CpG Island Methylator Phenotypes during Tumor Recurrence. Cell Rep. *23*,
939   637–651.

940   Tesileanu, C.M.S., van den Bent, M.J., Sanson, M., Wick, W., Brandes, A.A., Clement, P.M.,
941   Erridge, S.C., Vogelbaum, M.A., Nowak, A.K., Baurain, J.F., et al. (2021). Prognostic
942   significance of genome-wide DNA methylation profiles within the randomised, phase 3, EORTC
943   CATNON trial on non-1p/19q deleted anaplastic glioma. Neuro Oncol.

944   Touat, M., Li, Y.Y., Boynton, A.N., Spurr, L.F., Iorgulescu, J.B., Bohrson, C.L., Cortes-Ciriano, I.,
945   Birzu, C., Geduldig, J.E., Pelton, K., et al. (2020). Mechanisms and therapeutic implications of
946   hypermutation in gliomas. Nature 580, 517–523.

947   Triche, T.J., Weisenberger, D.J., Van Den Berg, D., Laird, P.W., and Siegmund, K.D. (2013).
948   Low-level processing of Illumina Infinium DNA Methylation BeadArrays. Nucleic Acids Res. *41*,
949   e90.

950 Turcan, S., Rohle, D., Goenka, A., Walsh, L.A., Fang, F., Yilmaz, E., Campos, C., Fabius,
951 A.W.M., Lu, C., Ward, P.S., et al. (2012). IDH1 mutation is sufficient to establish the glioma
952 hypermethylator phenotype. Nature *483*, 479–483.

953 van den Bent, M.J., Afra, D., de Witte, O., Ben Hassel, M., Schraub, S., Hoang-Xuan, K.,
954 Malmström, P.O., Collette, L., Piérart, M., Mirimanoff, R., et al. (2005). Long-term efficacy of
955 early versus delayed radiotherapy for low-grade astrocytoma and oligodendroglioma in adults:
956 the EORTC 22845 randomised trial. Lancet *366*, 985–990.

957 Varn, F.S., Johnson, K.C., Wade, T.E., Malta, T.M., Sabedot, T.S., Barthel, F.P., Kim, H.,
958 Ahmed, N., Datta, I., Barnholtz-Sloan, J.S., et al. (2021). Longitudinal analysis of diffuse glioma
959 reveals cell state dynamics at recurrence associated with changes in genetics and the
960 microenvironment. BioRxiv.

961 Weller, M., van den Bent, M., Preusser, M., Le Rhun, E., Tonn, J.C., Minniti, G., Bendszus, M.,
962 Balana, C., Chinot, O., Dirven, L., et al. (2021). EANO guidelines on the diagnosis and
963 treatment of diffuse gliomas of adulthood. Nat. Rev. Clin. Oncol. *18*, 170–186.

964 Wick, W., Hartmann, C., Engel, C., Stoffels, M., Felsberg, J., Stockhammer, F., Sabel, M.C.,
965 Koeppen, S., Ketter, R., Meyermann, R., et al. (2009). NOA-04 randomized phase III trial of
966 sequential radiochemotherapy of anaplastic glioma with procarbazine, lomustine, and vincristine
967 or temozolomide. J. Clin. Oncol. *27*, 5874–5880.

968 Wu, X., Liu, Y., Chen, X., Sun, Q., Tang, R., Wang, W., Yu, Z., and Xie, M. (2013). Involvement
969 of TREK-1 activity in astrocyte function and neuroprotection under simulated ischemia
970 conditions. J. Mol. Neurosci. 49, 499–506.

971 Yao, L., Shen, H., Laird, P.W., Farnham, P.J., and Berman, B.P. (2015). Inferring regulatory
972 element landscapes and transcription factor networks from cancer methylomes. Genome Biol.
973 *16*, 105.

974 Yu, L., Mikloucich, J., Sangster, N., Perez, A., and McCormick, P.J. (2003). MyoR is expressed
975 in nonmyogenic cells and can inhibit their differentiation. Exp. Cell Res. *289*, 162–173.

976 Zhang, Y., Maksimovic, J., Naselli, G., Qian, J., Chopin, M., Blewitt, M.E., Oshlack, A., and
977 Harrison, L.C. (2013). Genome-wide DNA methylation analysis identifies hypomethylated genes
978 regulated by FOXP3 in human regulatory T cells. Blood *122*, 2823–2836.
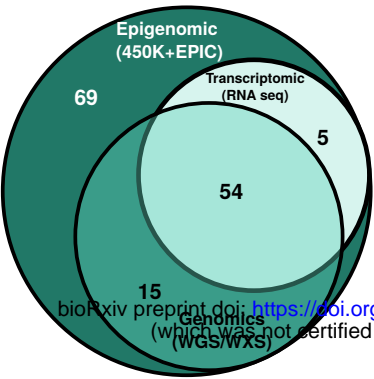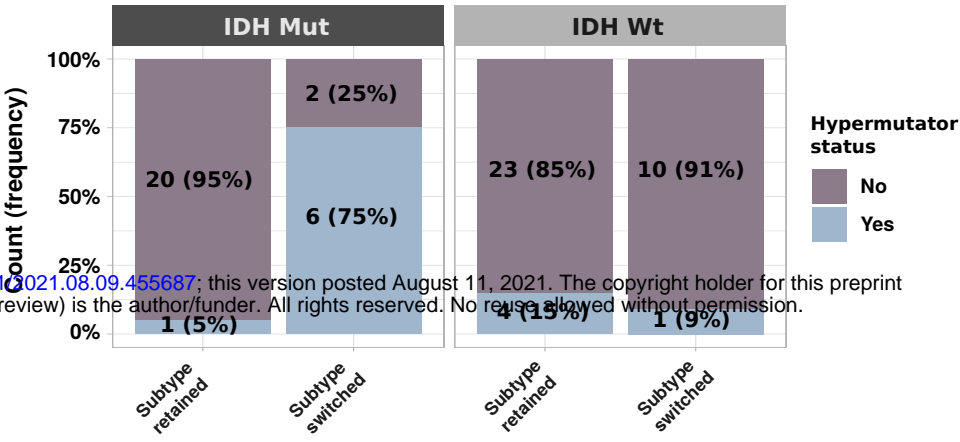
Figure 1. Epigenomic evolution of matched initial and recurrent gliomas. A) Venn diagram of number of patients who had DNA methylation, genomic (WGS/WXS) and/or RNAseq profiling. B) Clinical and molecular overview of matched initial and recurrent DNA methylation cohort. Each column represents a single patient (n=143) at two separate time points grouped by IDH status and ordered by increase of gain of DNA methylation at recurrent tumor from left-to-right. Top plot shows the surgical interval of each patient. C) Frequency of patients with hypermutator tumors that switched or retained molecular subtype at recurrence. Patients are divided by IDH status.

Figure 2. Master regulators associated with IDHmut glioma recurrence/progression. A) Circos plot diagram showing epigenomic changes between initial and recurrent IDHmut tumors. The outer track shows chromosome location. The second track shows genomic location of 1,590 differentially methylated CpG probes between initial and recurrent IDHmut tumors. Height of dots represents the difference of methylation levels between recurrent and initial. The third track shows the genomic location of H3H27ac peaks defined by differential binding analysis of IDHmut G-CIMP-high patients that progressed to G-CIMP-low. Height of the peaks represents the fold change of differential binding analysis. The fourth inner track shows the genomic location of the candidate genes epigenetically regulated by the CpG probes (yellow bars). Height of the bars represents the -log of FDR. Genes related to cell cycle are labeled. The top transcription factor (TF) binding motifs enriched among the candidate DMP are FOS/JUN family and NEUROD1, whose DNA signature motifs are represented in the center of the circos plot. B) Pathway analysis of epigenetically activated genes in recurrent IDHmut tumors. C) Gene expression levels of master regulator transcription factors (MRTFs) of IDHmut initial and recurrent tumors. IDHwt tumors are shown as a reference. D) Stemness activity in glioma samples stratified by primary/recurrent and IDH mutation status.
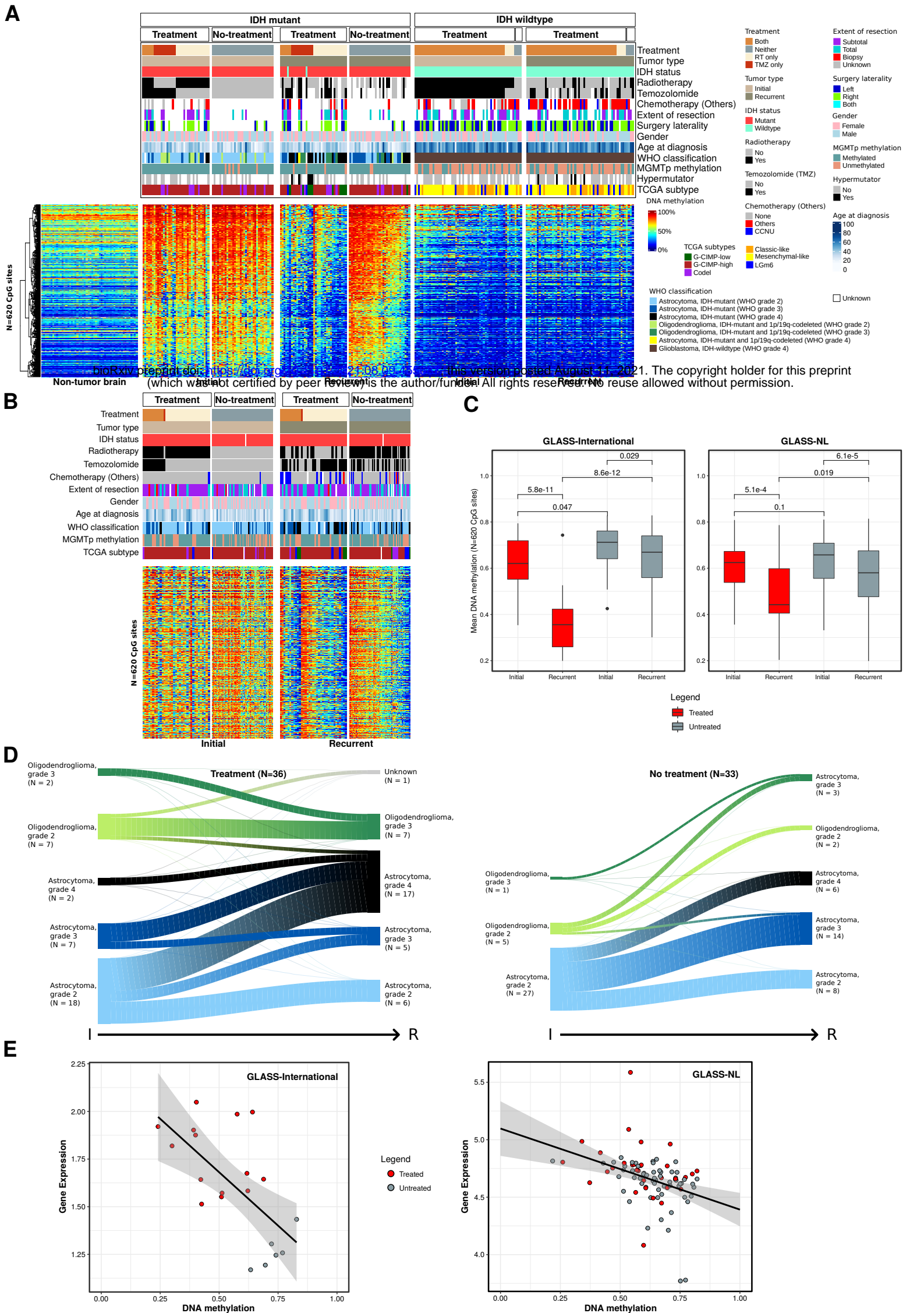
Figure 3. DNA methylation loss associates with malignant transformation of glioma after standard treatment. A) Heatmap of DNA methylation data. Supervised hierarchical clustering analysis of 620 CpG probes that are associated with different treatment strategies in IDH-mutant paired glioma samples. Columns represent glioma samples, rows represent CpG probes. Samples were stratified and clustered based on IDH mutation status and primary/recurrent status and CpGs were ordered using hierarchical clustering methods. Non-neoplastic brain samples are represented on the left of the heatmap. DNA methylation beta-values range from 0 (low) to 1 (high). Additional tracks are included at the top of the heatmaps to identify each sample membership within separate cluster analysis. B) Heatmap of DNA methylation data in the validation cohort - GLASS-NL, showing the same 620 CpG probes of panel A. C) Boxplot of the average DNA methylation beta-value of the 620 CpG probes from panel A. Samples are stratified by primary/recurrent status and by treated/non-treated status. Left: GLASS-International samples. Right: GLASS-NL samples. D) Evolution of tumor histology (2021 WHO classification) from primary to recurrent samples after treatment compared to non-treated gliomas. E) Scatter plot of mean DNA methylation of CpG probes and mean gene expression of the epigenetically regulated genes after treatment.
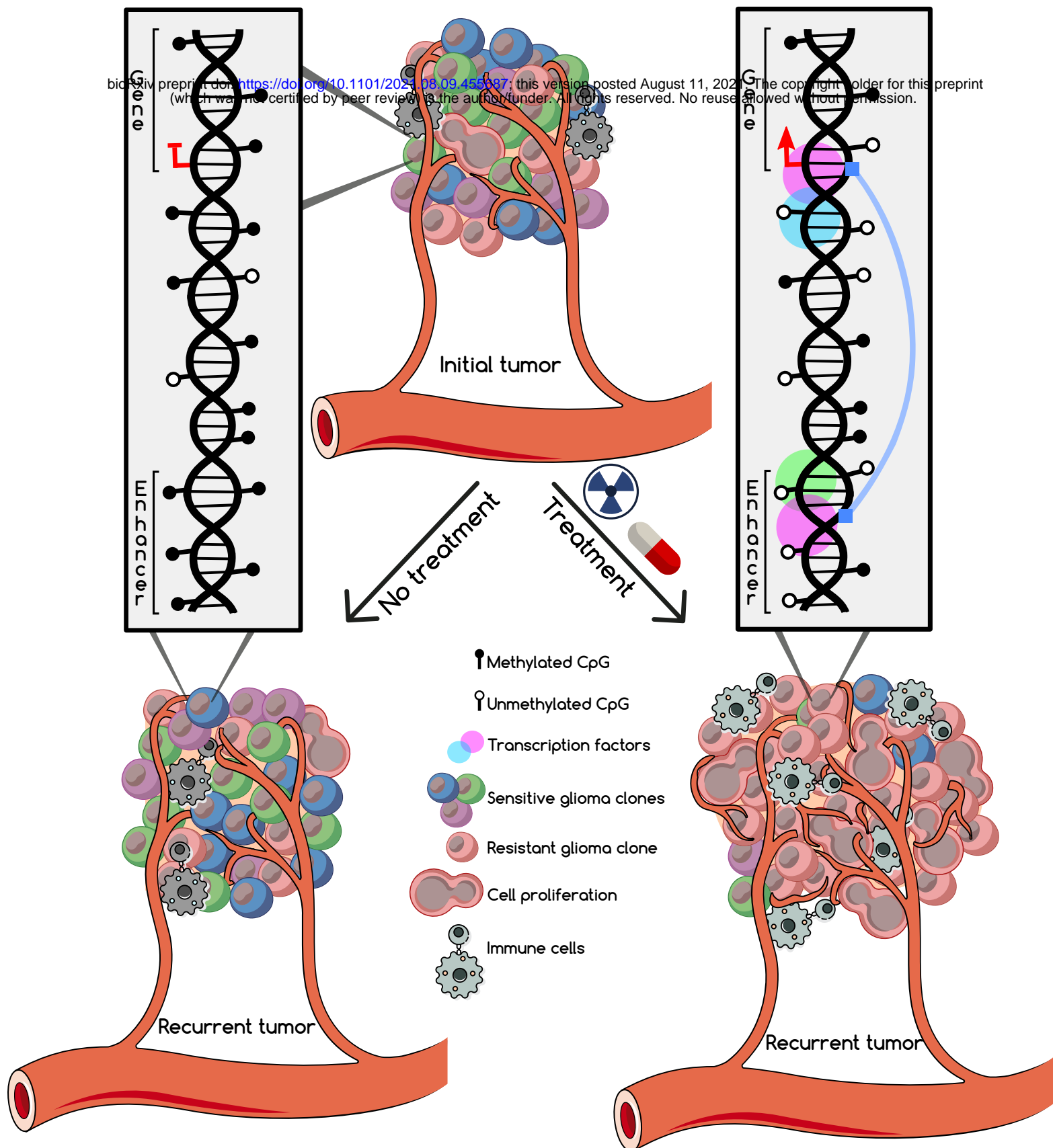
Figure 4. Tumor microenvironment and clinical implications of treatment in IDH-mutant gliomas. A) CD31 and CD8 proportions (range scaled from 0 to 100%) in samples originating from IDHmut matched initial and recurrent tumors in treated and non-treated patients. B) Illustrative immunohistochemical stainings for two marker proteins (CD31 and CD8) in an individual patient showing change of levels of tumor-infiltrating immune cells between initial and recurrent tumors. C/D) Overall survival and surgical interval analysis of IDHmut gliomas for the GLASS International (C) and GLASS-NL (D) cohorts.

Figure 5. Schematic of treatment-induced epigenetic activation of cell cycle in IDHmut recurrent tumors. Standard treatment induces loss of methylation in IDHmut tumors with further epigenetic activation of cell cycle related genes associated with early tumor progression. In IDHmut non-treated patients, epigenetic changes are much more limited and tumors may progress later, either spontaneously or after subsequent treatment.